Silk Microlens Array

Seung Ho Choi (seunghochoi@yonsei.ac.kr)
Yonsei University
Tien Son Ho
Yonsei University
Elijah Effah
Yonsei University
Ezekiel Edward Nettey-Oppong
Yonsei University
Seungyeop Choi
Yonsei University
Ji Hyeon Choi
Kyung Hee University
Byungjo Jung
Yonsei University
Sang Woo Lee
Yonsei University
Kee Young Kim
National Institute of Agricultural Sciences
Seong-Wan Kim
National Institute of Agricultural Sciences
Kyung Min Byun
Kyung Hee University

Research Article

Keywords: Optics, Silk microlens array, silk protein, biomaterials

Posted Date: January 5th, 2022

DOI: https://doi.org/10.21203/rs.3.rs-1222988/v1

Silk microlens array

Tien Son Ho[1,+], Elijah Effah[1,+], Ezekiel Edward Nettey-Oppong[1,+], Seungyeop Choi[1], Ji Hyeon Choi[2], Kee Young Kim[3], Seong-Wan Kim[3], Byungjo Jung[1], Sang Woo Lee[1], Kyung Min Byun[2,*], and Seung Ho Choi[1,*]

[1]Department of Biomedical Engineering, Yonsei University, Wonju 26493, Republic of Korea
[2]Department of Biomedical Engineering, Kyung Hee University, Yongin 17104, Republic of Korea
[3]Department of Agricultural Biology, National Institute of Agricultural Sciences, Rural Development Administration, Wanju 55365, Republic of Korea
*kmbyun@khu.ac.kr, seunghochoi@yonsei.ac.kr
[+]These authors contributed equally to this work

ABSTRACT

Optics that are capable of merging with biomaterials create a variety of opportunities for sensing disease, for therapeutics, and for augmenting brain-machine interface. The FDA has approved silk devices for sutures and reconstructive surgery. Recently, a silk product made from regenerated silk protein is FDA approved for orthopedic application, as the understanding of structure and processing technologies of silk fibroin has been improved. Here, we report a facile fabrication process to construct silk microlens array. The process includes preparation of regenerated silk solution and casting on a micropatterned poly(dimethylsiloxane) (PDMS) master. Due to the identical surface area of a unit patterned regime, the silk solution exhibits a partial wetting state in the vicinity of the silk solution–PDMS–vapor interface with same contact angle, and after drying, produces consistent radius of curvature within the microlens array. This in turn provides highly uniform focal length, focal spot diameter, and imaging performance of individual lens. Our results provide the foundation for biophotonic microlens adding new capabilities for implantable and degradable devices from regenerated silk protein.

Introduction

Over the years, there has been growing demand for biomaterial-based optical devices in biomedical optics. Lens, in particular, is a fundamental optical device and its biopolymer form is indispensable for implantable optical devices or biotic/abiotic interface between tissue and optics. For biomaterial-based lens, it is challenging to realize small, static, uniform curvilinear surfaces using biopolymer.

Typically, microlens are fabricated by direct and indirect methods[1]. In direct methods, the lens is obtained from the base material. For example, the material directly shapes into the lens by the surface tension of the liquid or thermoplastic state of the material[2-6]. Although the direct methods are simple, cost-effective, and favorable for realizing super smooth curved surface of lens, it is difficult to precisely control the shape and size of the microlens as the lens geometry is determined by wettability, time, temperature, and pressure. In indirect methods, the lens material is shaped from a mold. Such concave microlens molds are generally fabricated from microelectromechanical systems (MEMS) manufacturing technologies[7] and ultraprecision machining method[8]. Although the indirect methods can favorably control the shape of lens, these processes usually employ complex and harsh nanofabrication steps using acid or with high temperature/pressures. Thus, it is critical to find proper microlens fabrication techniques, which allow processing of biopolymers.

With advances in engineering, assembling, and synthesizing technologies, multifunctional biomedical devices have been realized through biopolymers such as collagen, chitosan, and silk fibroin. Among these biopolymers, silkworm silk of *Bombyx mori* has emerged as an ideal material for biophotonic devices[9-12] because of a number of attributes. Silkworm silk fibers are typically white (Fig. 1a) and show broadband reflection through optical scattering by disordered medium[13].

Silk fibroin is extracted from native silkworm silk; it is generally regarded as regenerated silk fibroin. This regenerated silk fibroin is typically aqueous form (Fig. 1b) that can be annealed and transformed into different configuration such as film. Once annealed, most of the secondary structures consists of antiparallel β-sheet (Fig. 1c) forming the bulk crystalline matrix for ordered structures. The crystallized silk films show superior transparency (Fig. 1d,e), high surface flatness, and high mechanical strength, all of optical and structural properties preferably suited for use as optical substrates[14-16]. It is known that the refractive index of the silk films[17] ranges from 1.54 to 1.58 (Fig. 1f).

Soft lithography is a simple yet effective top-down fabrication scheme for patterning silk fibroin film. By casting silk fibroin solution on patterned surfaces, micro/nano structures can be transferred to silk films. Using soft lithography, a variety of 2D and 3D optical devices have been realized on free-standing silk film that includes holographic surface and diffraction grating[9,14,15]. This fabrication technique minimizes harsh nanofabrication steps using acid or with high temperature/pressures, as the secondary structure of silk fibroin is vulnerable to temperature, mechanical shear, and ionic strength[18]. This allows cost-effective, eco-friendly, and sustainable production of the silk-based biomedical device. However, for soft lithography, it is challenging to obtain smooth and uniform curved surface of master molds[19,20].

In this study, we hybridized direct and indirect methods of microlens fabrication for a simple yet efficient fabrication of silk microlens array; we used a patterned mold to achieve consistent contact angle of silk solution droplet such that the droplet dries to form uniform silk microlens. We extracted silk fibroin solution and casted on a micropatterned poly(dimethylsiloxane) (PDMS) microwell array to pattern silk fibroin film into microlens array. At the vicinity of the silk solution–PDMS–vapor interface, the silk solution exhibits intermediate wetting state. This partial wetting state makes a super smooth curved surface of the silk solution within the microwell array. Due to the identical surface area of a unit patterned regime, the unit silk droplet of partial wetting state experiences a uniform contact angle at the vicinity of the silk solution–PDMS–vapor interface inside the PDMS microwell array. Through this approach, we obtained uniform plano-convex silk microlens array with consistent lens diameter and

radius of curvature over the entire area of the device (3 cm × 3 cm). We further confirmed that such lens structures are consistent among different devices. To investigate the optical and imaging performance of silk microlens array, we further characterized the focal length, focal spot diameter, and depth-of-field and compared these characteristics between individual microlens.

Results

Fabrication of silk microlens array

Figure 1g shows a schematic of the direct and indirect hybridized method of microlens fabrication for silk microlens array. In this hybridized method, we combined soft lithography with a casting process such that the patterned mold achieves uniform diameter and contact angle of silk solution droplet. The process of fabricating silk microlens array consists of two major steps: the fabrication of PDMS microwell array (red line in Fig. 1g) and the extraction of regenerated silk fibroin solution from *Bombyx mori* cocoons (grey line in Fig. 1g)[21].

For the fabrication of PDMS microwell array, a SU-8 negative photoresist is spin coated on a pre-cleaned silicon wafer. UV light (365 nm) is exposed through a patterned shadow mask to form positive SU-8 master. By casting PDMS on the positive SU-8 master, a PDMS microwell array is replicated.

For the extraction of regenerated silk fibroin solution, white silk cocoons were cut into small pieces. In its native form, a gum-like layer of sericin covers two singular filaments of fibroin, and sericin should be removed to eliminate undesirable immune responses when fabricating silk-based devices[22]. To remove sericin, the silk cocoon is boiled in 0.02 M aqueous solution of sodium carbonate for 30 min. The sericin-free fibers are dissolved in aqueous solution of lithium bromide at 60 °C. The subsequent dialysis removes the lithium bromide and yields a 7 wt% regenerated silk fibroin solution. Casting regenerated silk fibroin solution on the PDMS microwell array creates silk microlens array.

Structure of silk microlens array

Figure 2a shows the appearance of fabricated silk microlens array and bare silk film. Through the bare silk film, the “YONSEI UNIVERSITY” logo is clearly imaged. Through the silk microlens array, the logo appears to divide into pixels; when the ‘TY’ portion of the logo is magnified, it reveals the microlens array.

In Fig. 2b, a side view image shows smooth curved surface of the lens with 200 μm diameter; the radius curvature of the lens was fit to be 152 μm. Over the entire area of the device (3 cm × 3 cm), silk microlens array has consistent lens diameter (Fig. 2c and Fig. 2d) from lens to lens. Figure 2e shows the representative curvature profiles of lens (inset of Fig. 2c), which were calculated from the circular fit. For seven different profiles, the radius of curvatures and lens heights were determined to be (154.0 μm and 36.8 μm), (153.1 μm and 36.6 μm), (152.1 μm and 36.3 μm), (152.2 μm and 36.4 μm), (155.5 μm and 35.59 μm), (155.0 μm and 35.4 μm), and (153.9 μm and 36.8 μm), showing high structural consistency within a single device.

Also, it is important to note that such lens structures are consistent among different devices. For five different microlens devices, the average radii of curvature were 152.3 μm, 152.5 μm, 152.5 μm, 152.9 μm, and 152.9 μm (Fig. 2f). Each device has a standard deviation of 1.33 μm, 0.93 μm, 1.03 μm, 0.83 μm, and 1.14 μm. Such consistent radius of curvatures and their low standard deviations confirm that our soft-lithography-based casting process produces highly consistent microlens array.

To obtain the desired thickness of silk microlens substrate, we controlled the initial thickness of silk fibroin solution. Figure 2g shows the relation between the initial thickness of silk solution d_i and the thickness of dried silk film d_{dry}. The initial thickness of the silk solutions typically decreased to 7% upon drying. To determine the surface quality, we employ atomic force microscopy (AFM) to reveal the

surface morphology of dried silk substrate (Fig. 2h). The dried silk substrate has high surface quality such that the root-mean-square value of the surface profile is 1.5 nm.

Physical mechanism of curvature formation of silk microlens array

To understand how the silk solution form a consistent curvature of droplet within microwell array, we analyzed the wetting state of the silk solution at the silk solution–PDMS microwell interface. From the macroscopic viewpoint, the wettability of a liquid is evaluated by contact angle (Fig. 3a). On an ideally flat surface, the contact angle θ_Y is determined by Young's equation:

$$\cos\theta_Y = \frac{\gamma_{sv} - \gamma_{sl}}{\gamma_{lv}} \quad (1)$$

where γ_{sv}, γ_{lv}, and γ_{sl} are the surface tension of the solid–vapor, liquid–vapor, and solid–liquid interfaces, respectively. On hierarchical micro-structured surfaces, the wettability of a liquid is described by partial wetting model[23],

$$\cos\theta = \Phi_{sl}\cos(\theta_Y) + \Phi_{lv}\cos 180^{\circ} \quad (2)$$

where Φ_{lv} and Φ_{sl} are the area ratio of the liquid–vapor and solid–liquid interface to the flat surface, respectively (Fig. 3g). This intermediate wetting state exist between fully-wetted state of Wenzel model and non-wetted stat of Cassie–Baxter model (Fig. 3b).

As PDMS is well known for its hydrophobic surface, bare PDMS film is difficult to wet with a distilled water (water contact angle of $\theta_Y = 107^{o}$) and such hydrophobicity is further enhanced on micro-structured PDMS ($\theta = 112^{o}$) (Fig. 3c). The increase of water contact angle indicates that the micro-structures reduce the solid–vapor surface tension γ_{sv} of bare PDMS film from 18.8 mJ/m^2 to 15.9 mJ/m^2. Compared to distilled water, PDMS is easier to wet with silk solution for both unmodified surface ($\theta_Y = 81.6^{o}$) and micro-structured surface ($\theta = 88.2^{o}$) (Fig. 3d); at liquid–vapor interface, the surface tension of the silk solution (γ_{lv} = 47 mJ/m^2) is smaller than that of the distilled water (γ_{lv} = 72.8 mJ/m^2) (Fig. 3e). As a result, the silk solution is prone to form intermediate wetting state inside of microwell array (Fig. 3f).

In Figure 3f, the silk solution creates a concave surface structure through the intermediate wetting state. Within the microwell array, the intermediate wetting state has the solid–liquid, liquid–vapor, and solid–vapor interfaces as shown in Fig. 3g. In this state, the consistent contact angle of silk solution droplet θ is manifested by the consistent γ_{sv}, γ_{lv}, $\gamma_{sl,}$ Φ_{lv}, and Φ_{sl} in equations (1) and (2). Interfacial surface tensions γ_{sv}, γ_{lv}, and γ_{sl} are constituent material properties of the silk solution, PDMS, and air; thus, γ_{sv}, γ_{lv}, γ_{sl}, and θ_Y are uniform over the PDMS microwell array. Because of the uniform size of microwell, the area ratio of the liquid–vapor interface Φ_{sl} and the area ratio of the solid–liquid interface Φ_{lv} are preserved within the PDMS microwell array (Fig. 3h); Φ_{lv}, and Φ_{sl} can be preserved even for different volumes of casting solution. Due to the identical surface area of a unit patterned regime, the unit silk droplet of partial wetting state experiences a uniform contact angle θ at the vicinity of solid–vapor–liquid interface. Thus, the PDMS microwell array achieves a consistent contact angle of silk solution droplet such that the droplet dries to form a super smooth curved surface of silk microlens.

Through this approach, we obtained uniform plano-convex silk microlens array with consistent lens diameter and radius of curvature over the entire area of the device (3 cm × 3 cm). Importantly, our soft-lithography-based casting process is simple yet intrinsically robust to the volume mismatch of casting solution and allows consistent lens structures among different devices.

Optical characteristics of silk microlens array

To investigate the optical properties of silk microlens array, we characterized the focal length and focal spot diameter, and compared these characteristics for individual microlens. The collimated laser beam (λ = 543.5 nm) was illuminated on the surface of the silk microlens array, and the transmission intensity was measured using a microscopy imaging setup (Fig. 4a). Figure 4b shows the transmission intensity at the focal plane of the silk microlens arrays. The sharp focused beam spots with a diameter ~ 2.89 µm are clearly observed for hexagonal arrangement of microlens.

The focal length was characterized by translating the silk microlens array along the optical axis of the microscope imaging system (z-axis) with a unit translation step of 1 µm; Figure 4c shows the represented optical sections at different translation distances. By stacking multiple optical sections, we reconstructed the 3D beam profile. In Figure 4d, the top view (x-z plane) of beam profile shows that the incident light is focused on to a single spot at the distance of ~ 265 µm. Using the finite element method (FEM), we performed the full-wave simulations (Fig. 4e). For FEM computation, we modeled a silk microlens with an axially symmetric plano-convex lens of 50 µm diameter and 2.09 µm height, which were extracted from the curvature profiles shown in Fig. 2e. In Figure 4e, the electric field amplitude $|E|$ is focused at the distance of ~ 262.4 µm; the measured beam profile (Fig. 4d) and the full-wave simulation (Fig. 4e) are in good agreement. In theory, the focal length is described by

$$f = \frac{r^2 + h^2}{2h(n-1)} \tag{3}$$

where f is the focal length, n is the refractive index of silk fibroin, r and h are the radius and height of the lens, respectively. This returns the theoretical focal length of 269.5 µm; the measured focal length agrees well with the results of theory and simulation. From the measured focal length, we can obtain the half of the focusing angle θ that yields the numerical aperture NA = $n_0 \sin\theta$ (where n_0 is the refractive index of the background) of 0.35. At the focal plane, the beam spot has a diameter of 2.89 µm (Fig. 4f), which agrees well with the simulation result of 2.6 µm (Fig. 4g).

Through soft-lithography-based casting process approach, we obtained uniform plano-convex silk microlens array with consistent focal length (Fig. 4h) and focal spot diameter (Fig. 4i). The optical and structural properties of the fabricated silk microlens array are summarized in Table 1.

To investigate imaging performance of silk microlens array, we imaged 1951 USAF resolution test target using the silk microlens array. Figure 5a shows the schematic of the optical microscope imaging setup with the silk microlens array. White light was illuminated on the resolution test target, which was precisely placed to align with the silk microlens array. Figure 5b and 5c present the bright-field images generated through the planar surface of silk microlens and the curved surface of silk microlens, respectively. Such imaging capability of the silk microlens was further confirmed in Fig. 5d, e that the silk microlens is integrated with higher magnification of objective lens.

Discussion

In conclusion, we report a new method for fabricating smooth curved surfaces of silk microlens with uniform curvature. The significance of our fabrication method is better captured when the nature of silk fibroin is well understood. The secondary structure of silk fibroin is vulnerable to temperature, mechanical shear, and ionic strength[18]. Thus, most of classical microlens fabrication techniques, which require harsh nanofabrication steps, are hardly applicable to silk fibroin. As one of the top-down approaches, soft lithography had been used to obtain silk-based optical components such as holographic surface and diffraction grating[9,14,15]. However, it is challenging to obtain smooth and uniform curved surface of master molds.

In our new method, we took advantage of distinct properties of the liquid phase and the solid crystal of silk fibroin. In the liquid phase, the silk solution is favorable to shape into the super smooth curved surfaces by the surface tension inside the PDMS microwell array. Since the surface tension of the silk solution is smaller than that of the distilled water, the silk solution is prone to form intermediate wetting state within the PDMS microwell. In principle, the size and shape of lens are determined by the micropatterned PDMS microwell array, instead of the surface tension of the liquid itself. When silk protein is annealed, most of the secondary structures are crystallized forming solid and consistent curved surface of lens. In realizing consistent lens structures, our soft-lithography-based casting process is intrinsically robust to the volume mismatch of casting solution. This allows a facile avenue for creating highly consistent lens structures, focal length, focal spot diameter, numerical aperture, and imaging performance within a device and among different microlens devices. Furthermore, this advancement provides a new enabling platform for emerging field of implantable and degradable microsystems from regenerated silk protein.

Methods

Silk fibroin extraction. *Bombyx mori* silkworm cocoons were purified by removing glue-like sericin proteins, as sericin is known to induce inflammatory responses. Silkworm cocoons were cut into small size pieces and boiled in an aqueous solution of 0.02 M sodium carbonate at 100℃ for 30 min. The boiled cocoons are rinsed in deionized water for 20 minutes and excess water is squeezed out; this process is repeated three times. The fibroin bundle is then dried overnight at room temperature. After drying, the fibroin bundle is dissolved in 9.3 M LiBr solution at 60℃ for 4 hours. The resulting solution is filtered with a membrane cloth to remove impurities. Water-based dialysis is conducted for three days to extract pure silk fibroin solution from the filtered solution. The filtered solution is injected into a dialysis membrane tube (12-14 kDa MWCO, Fisher Scientific), and then dialyzed against DI water at 5℃. At this stage, DI water is changed periodically over the three days period. The extracted solution is then centrifuged at 900 rpm for 20 minutes resulting in 7-8% (wt/vol) pure silk fibroin solution.

Photo-patterning of silicon wafer. The SU-8 master mold is fabricated by standard photolithography techniques. A silicon wafer is pre-cleaned with acetone, isopropanol, deionized water and piranha solution (a mixture of 100 ml H_2O_2 and 50 ml H_2SO_4). The cleaned wafer is then air-dried with a nitrogen gun and further dried on a hot plate at 120 ℃. Prior to SU-8 negative photoresist (SU-8 2050, Microchem) coating, the dried wafer is coated with hexamethyldisilazane (HMDS) in a vacuum chamber for 30 minutes. This is to ensure proper adhesion of SU-8 resist. 4 mL of SU-8 resist is dispensed on wafer and spin coated at 500 rpm for 10 seconds and accelerated to 1500 rpm for 30 seconds, to form a film of about 150 µm thickness. The SU-8 film is pre-baked at 65 ℃ for 5 minutes and further baked at 95 ℃ for 10 minutes to completely remove solvent in the film. Subsequently, the SU-8 film is patterned by exposure to UV light (MDA-400M) through a patterned shadow mask at 20 mW/cm^2 power for 60 seconds. After exposure, the wafer is post-baked at 65 ℃ for 5 minutes and further baked at 95 ℃ for 15 minutes to thermally initiate the cross-linking reaction. The SU-8 film is then sonicated with SU-8 developer for 2 minutes to create the pattern.

Fabrication of silk microlens array. Silk microlens array is constructed by casting silk fibroin solution on a PDMS microwell array. To mold PDMS on the SU8 master, PDMS pre-polymer and curing agent were mixed with ratio of 10:1, respectively. The PDMS is carefully poured onto the SU8 master mold and cured at 60 ℃ for 2 hours. After curing, the PDMS microwell array is gently detached from the SU8 master mold with tweezers. The silk microlens array is then formed by casting silk fibroin solution on the PDMS microwell array. During the casting process, 400µL – 1mL of silk fibroin solution is carefully poured on the PDMS microwell array. The solution is allowed to dry in ambient temperature for 18 hours. After complete drying, the silk microlens array is gently peeled off from the PDMS microwell array.

Surface tension calculations. To quantitatively evaluate the surface free energy of PDMS and silk solution droplet, we used an equation of state of interfacial tensions[24];

$$\cos\theta = -1 + 2\sqrt{\frac{\gamma_{sv}}{\gamma_{lv}}}e^{-\beta(\gamma_{sv}-\gamma_{lv})^2}, \quad (4)$$

where θ is the contact angle, γ_{sv} is the solid-vapour surface tension, and γ_{lv} is the liquid-vapor surface tension. γ_{lv} of water is known to be 72.8 mJ/m^2 and β has been empirically computed as 0.001247 (mJ/m^2)$^{-2}$[17]. With a measured θ of water, the γ_{sv} of bare PDMS and PDMS microwell are determined to be 18.83 mJ/m^2 and 15.94 mJ/m^2, respectively. We further derive γ_{lv} of silk solution droplet from the following known parameters: γ_{sv} of PDMS and β. This returns γ_{lv} of silk solution droplet on bare PDMS and PDMS microwell as 47.05 mJ/m^2 and 47.07 mJ/m^2, respectively.

Focal length and spot measurements. To characterize the optical characteristics of the silk microlens array, a collimated laser beam (λ = 543.5 nm) is incident on a hexagonal arrangement of microlens for a plane wave illumination. The transmission intensity is imaged using a customized microscopy imaging setup.

Full-wave simulation using FEM. For FEM computation, we modeled a silk microlens with an axially symmetric plano-convex lens of 50 μm diameter and 2.09 μm height, which were extracted from the curvature profiles shown in Fig. 2e. The refractive index of the regenerated silk protein was set to 1.5565 for 543.5 nm wavelength[25]. The silk microlens was applied to the 50 μm × 300 μm computational domain, which made it possible to fully simulate propagation of plane wave to the focal plane. We performed FEM analysis with the Wave Optics Module of COMSOL Multiphysics (5.3a version), in a manner similar to a previous work[13]. 2D Helmholtz equation was discretized to obtain E_z, H_x, and H_y components of the transverse magnetic (TM) mode. For the boundary conditions, the scattering boundary condition surround the computational domain.

References

1 Yuan, W., Li, L. H., Lee, W. B. & Chan, C. Y. Fabrication of Microlens Array and Its Application: A Review. *Chin J Mech Eng-En* **31**, (2018).

2 Sung, Y. L., Garan, J., Hu, Z. Y., Shan, X. N. & Shih, W. C. Modeling the surface of fast-cured polymer droplet lenses for precision fabrication. *Appl Optics* **57**, 10342-10347, (2018).

3 Zang, Z. G., Tang, X. S., Liu, X. M., Lei, X. H. & Chen, W. M. Fabrication of high quality and low cost microlenses on a glass substrate by direct printing technique. *Appl Optics* **53**, 7868-7871, (2014).

4 Wang, W. W. *et al.* Large-scale microlens arrays on flexible substrate with improved numerical aperture for curved integral imaging 3D display. *Sci Rep-Uk* **10**, (2020).

5 Chronis, N., Liu, G. L., Jeong, K. H. & Lee, L. P. Tunable liquid-filled microlens array integrated with microfluidic network. *Opt Express* **11**, 2370-2378, (2003).

6 Song, Y. M., Bae, S. Y., Yu, J. S. & Lee, Y. T. Closely packed and aspect-ratio-controlled antireflection subwavelength gratings on GaAs using a lenslike shape transfer. *Opt Lett* **34**, 1702-1704, (2009).

7 Albero, J. *et al.* Fabrication of spherical microlenses by a combination of isotropic wet etching of silicon and molding techniques. *Opt Express* **17**, 6283-6292, (2009).

8 Zhang, X. D., Fang, F. Z., Yu, L. H., Jiang, L. L. & Guo, Y. W. Slow slide servo turning of compound eye lens. *Opt Eng* **52**, (2013).

9 Huang, W. W., Ling, S. J., Li, C. M., Omenetto, F. G. & Kaplan, D. L. Silkworm silk-based materials and devices generated using bio-nanotechnology. *Chem Soc Rev* **47**, 6486-6504, (2018).

10 Li, C. M. *et al.* Design of biodegradable, implantable devices towards clinical translation. *Nat Rev Mater* **5**, 61-81, (2020).

11 Choi, J. H. *et al.* Combination of Porous Silk Fibroin Substrate and Gold Nanocracks as a Novel SERS Platform for a High-Sensitivity Biosensor. *Biosensors-Basel* **11**, (2021).
12 Kim, S. *et al.* Random lasing from structurally-modulated silk fibroin nanofibers. *Sci Rep-Uk* **7**, (2017).
13 Choi, S. H. *et al.* Anderson light localization in biological nanostructures of native silk. *Nat Commun* **9**, (2018).
14 Perry, H., Gopinath, A., Kaplan, D. L., Dal Negro, L. & Omenetto, F. G. Nano- and micropatterning of optically transparent, mechanically robust, biocompatible silk fibroin films. *Adv Mater* **20**, 3070-3072, (2008).
15 Parker, S. T. *et al.* Biocompatible Silk Printed Optical Waveguides. *Adv Mater* **21**, 2411-+, (2009).
16 Amsden, J. J. *et al.* Spectral analysis of induced color change on periodically nanopatterned silk films. *Opt Express* **17**, 21271-21279, (2009).
17 Perotto, G. *et al.* The optical properties of regenerated silk fibroin films obtained from different sources. *Appl Phys Lett* **111**, (2017).
18 Shimanovich, U. *et al.* Silk micrococoons for protein stabilisation and molecular encapsulation. *Nat Commun* **8**, (2017).
19 Lee, J. H. *et al.* High-Identical Numerical Aperture, Multifocal Microlens Array through Single-Step Multi-Sized Hole Patterning Photolithography. *Micromachines-Basel* **11**, (2020).
20 Kim, H. M., Kim, M. S., Lee, G. J., Yoo, Y. J. & Song, Y. M. Large area fabrication of engineered microlens array with low sag height for light-field imaging. *Opt Express* **27**, 4435-4444, (2019).
21 Rockwood, D. N. *et al.* Materials fabrication from Bombyx mori silk fibroin. *Nat Protoc* **6**, 1612-1631, (2011).
22 Thurber, A. E., Omenetto, F. G. & Kaplan, D. L. In vivo bioresponses to silk proteins. *Biomaterials* **71**, 145-157, (2015).
23 Nagayama, G. & Zhang, D. J. Intermediate wetting state at nano/microstructured surfaces. *Soft Matter* **16**, 3514-3521, (2020).
24 Yang, L. *et al.* Effect of Surface Free Energy on PDMS Transfer in Microcontact Printing and Its Application to ToF-SIMS to Probe Surface Energies. *Langmuir* **25**, 5674-5683, (2009).
25 Bucciarelli, A. *et al.* A comparative study of the refractive index of silk protein thin films towards biomaterial based optical devices. *Opt Mater* **78**, 407-414, (2018).

Acknowledgements

This work was carried out with the support of "Cooperative Research Program for Agriculture Science & Technology Development (Project No. PJ015373)" Rural Development Administration, Republic of Korea. This work was also supported by the fund of National Research Foundation of Korea (2019R1A2C2091068).

Author contributions

S.H.C. and K.M.B. mainly formulated the experimental designs and analyzed the data. T.S.H., E.E., E.E.N.O., S.C., J.H.C., S.W.L., S.W.K., and K.Y.K. prepared the silk specimens and fabricated the microlens array. T.S.H., E.E., B.J., and S.H.C. conducted the optical and imaging experiments. K.M.B. and S.H.C. conceived the idea and directed the research. E.E., K.M.B., and S.H.C. mainly wrote the manuscript. All of the authors discussed the results.

Competing interests

The author(s) declare no competing interests.

Figure captions

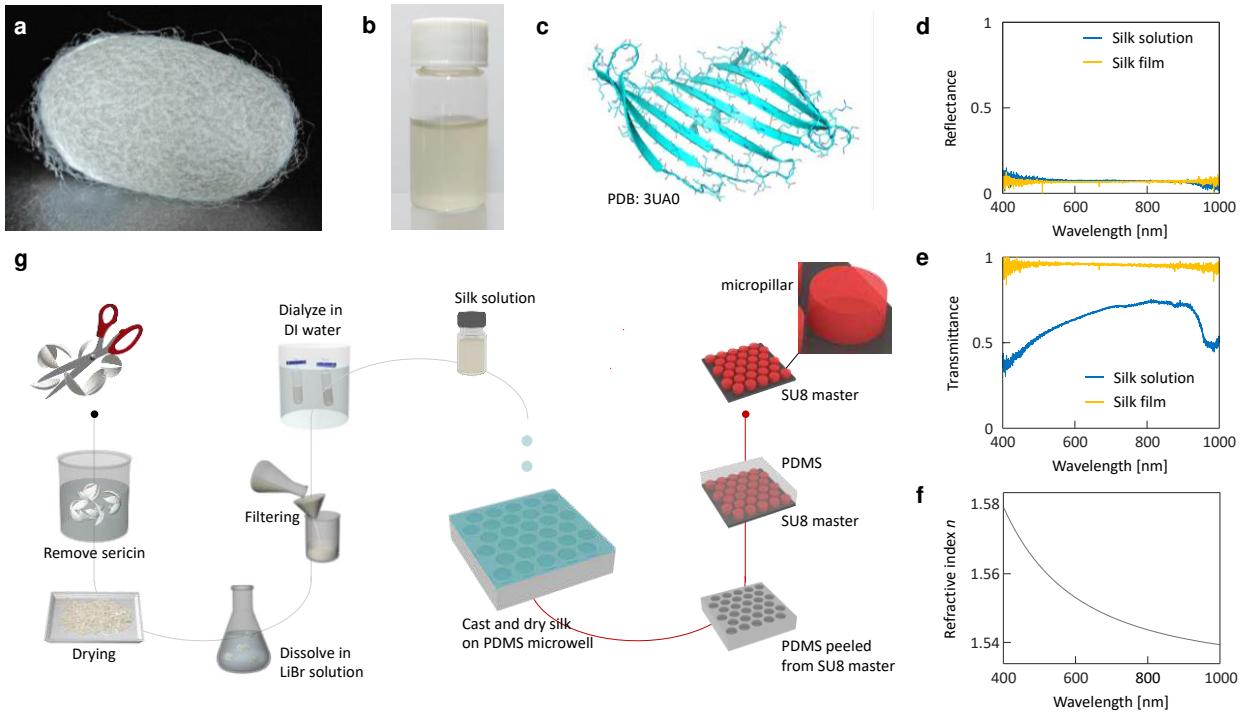

Figure 1. Optical characteristics of native and regenerated silk and fabrication procedure of silk microlens array. a Photograph of white silkworm silk cocoon of *Bombyx mori*. **b** Photograph of regenerated silk fibroin solution. **c** Molecular structure of β-sheet nanocrystal (PDB: 3UA0). **d**,**e** Transmittance and reflectance of silk fibroin solution and silk fibroin film with a thickness of ~ 50 μm. **f** Refractive index of silk fibroin film[17]. **g** Steps for fabricating silk microlens array; from extracting silk fibroin solution to aqueous casting for patterning silk fibroin microlens array. Silk fibroin extraction (as depicted in grey line) proceeds by cutting Bombyx mori cocoons into small pieces, removing sericin, drying fibroin bundle, dissolving silk fibroin fiber in 9.3M LiBr solution, filtering solution with membrane cloth, dialyzing filtered solution in deionized water, and centrifuging to obtain 7-8% (wt/vol) pure silk fibroin solution. PDMS microwell patterning (as depicted in red line) proceeds by spin coating SU-8 negative resist on pre-cleaned silicon wafer, UV light (365 nm) exposure through a patterned shadow mask to form positive SU-8 master, casting PDMS on positive SU-8 master, and peeling off negative PDMS microwell array. Cast and dry silk fibroin solution on PDMS microwell array.

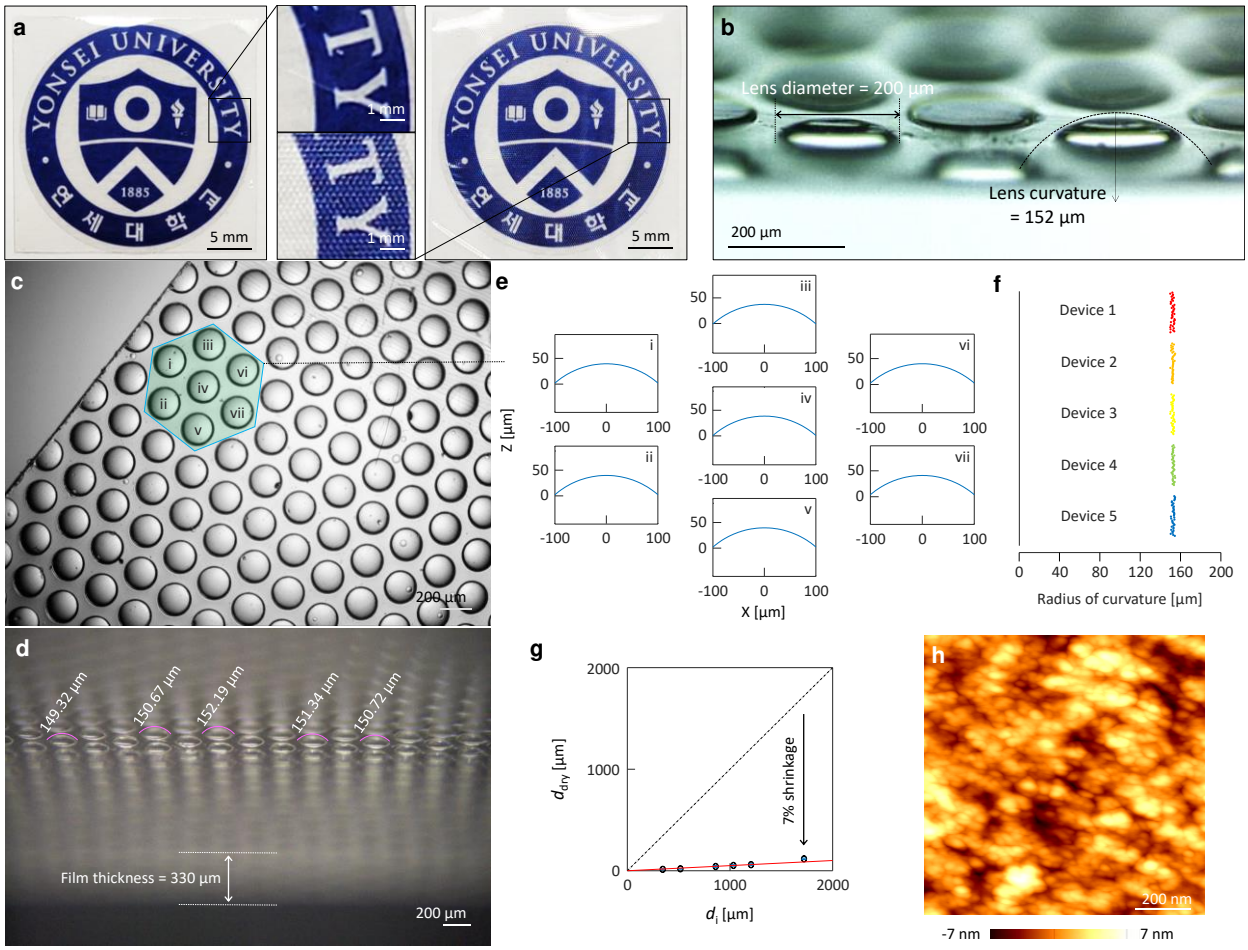

Figure 2. Structure of silk microlens array. a Photographs of bare silk film (left) and silk microlens array (right). While the "YONSEI UNIVERSITY" logo is clearly imaged through the bare silk film, the image appears to divide into pixels through the silk microlens array. The magnified 'TY' portion of the logo (middle) reveals the microlens array. **b** Side view image of microlens array showing plano-convex lens shape. Lens diameter and radius of curvature are 200 µm and 152 µm, respectively. **c** Top view image of microlens array. Inset depicts hexagonal arrangements of microlens. **d** Side view image showing film thickness of 300 µm and radius of curvature of five selected lens. **e** Curvature profiles of lens shown in inset of (c). **f** Radius of curvatures of microlens for five different silk microlens devices. **g** Relation between the initial thickness of silk solution d_i and the thickness of dried silk film d_{dry}. **h** AFM image of the silk microlens surface over an 1 µm × 1 µm area. The surface roughness (i.e. root-mean-square value of surface profile) is 1.5 nm.

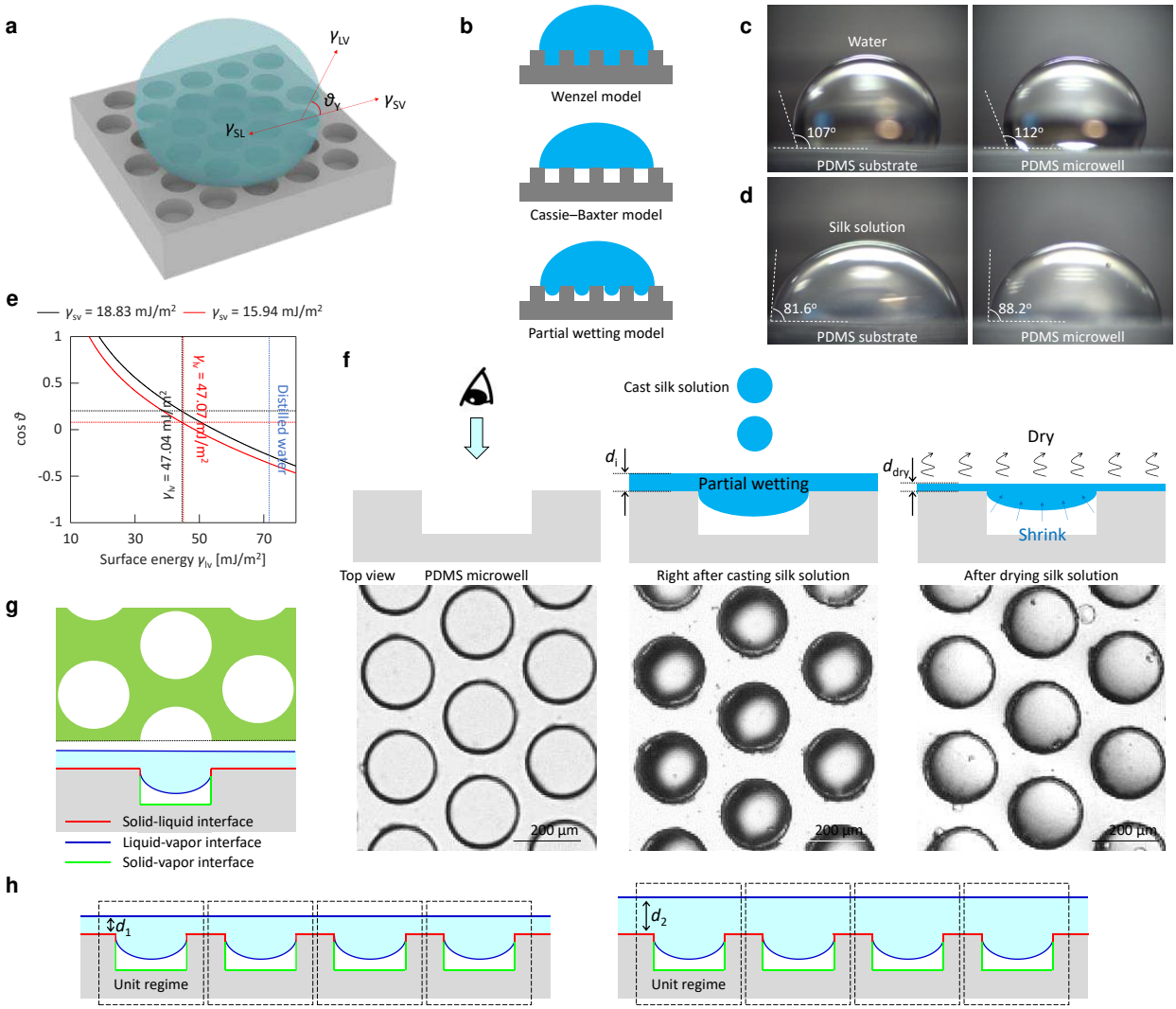

Figure 3. Physical mechanism of curvature formation of silk microlens array. a Contact angle for the silk solution droplet on a micro-structured surface. **b** Fully wetted Wenzel state (top), non-wetted Cassie-Baxter state (middle), and intermediate wetting state (bottom). **c, d** Contact angles of distilled water droplet (**c**) and silk solution droplet (**d**) on bare PDMS film (left) and PDMS microwell array (right). **e** γ_{lv} of the silk solution. **f** Top view image of PDMS microwell array before casting (left), after casting (middle), and after drying (right) silk solution. The silk solution is dried overnight at room temperature for 24 hour. **g** Red, blue, and green lines indicate solid-liquid, liquid-vapor, and solid-vapor interfaces inside of microwell array, respectively. **h** Solid-liquid, liquid-vapor, and solid-vapor interfaces of a unit microwell regime. Since different volume of casting solution merely changes the height from d_1 (left) to d_2 (right), the area ratio of the liquid–vapor interface Φ_{lv} and solid–liquid interface Φ_{sl} are preserved.

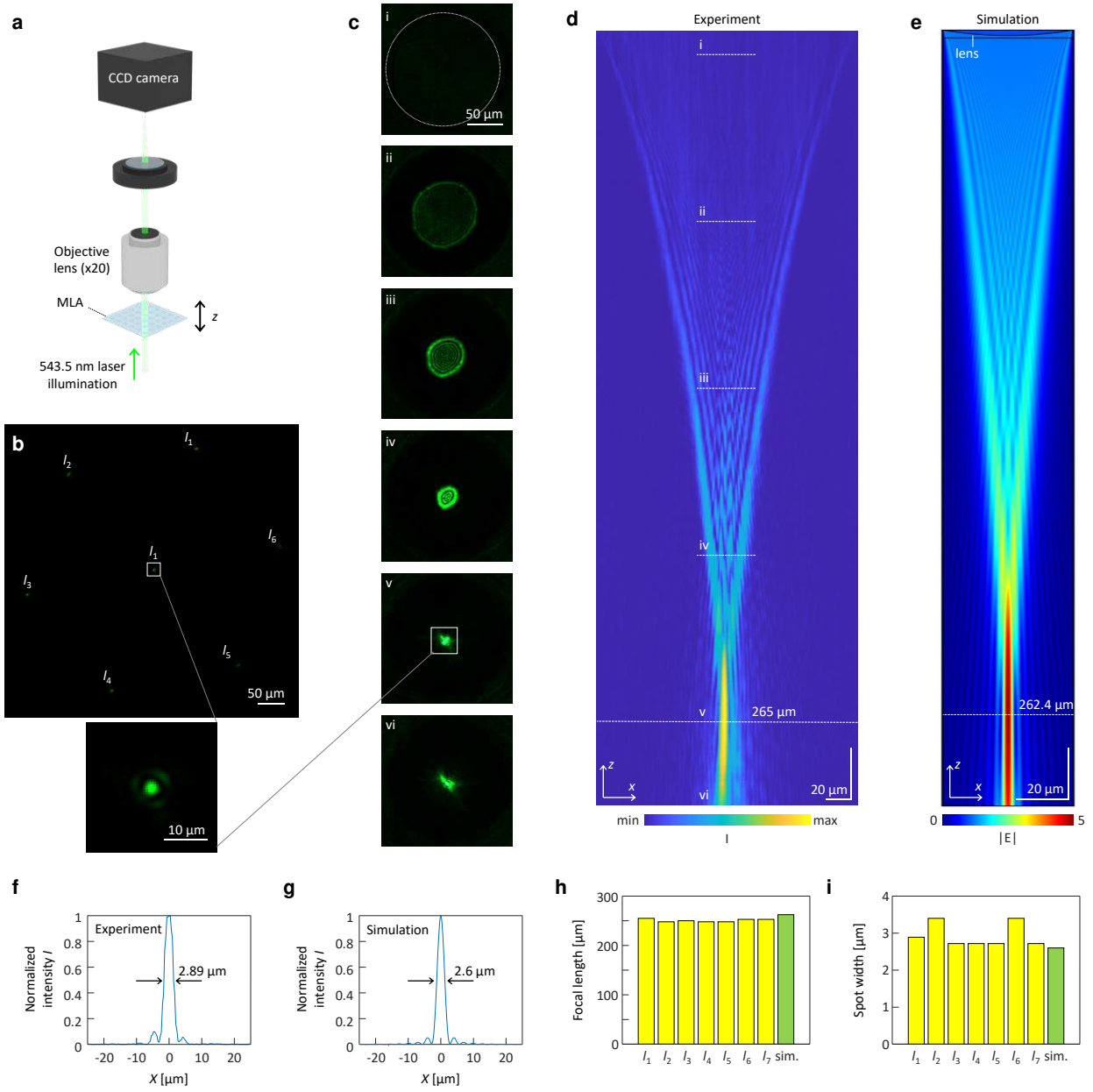

Figure 4. Optical characteristics of silk microlens array. a Schematic of microscopy imaging setup for focal length and focused beam spot measurement. **b** Beam profile at the focal plane of the silk microlens arrays. **c** Represented optical sections at different translation distances of silk microlens array. **d**, **e** Measured (**d**) and simulated (**e**) beam profile showing that the incident wave is focused onto a single spot. The simulation result displayed the electric field amplitude $|E|$. **f**, **g** Measured optical intensity (**f**) and simulated electric field intensity $I = |E|^2$ profile (**g**) along the white lines marked in (**d**) and (**e**), respectively. **h**, **i** Focal length (**h**) and focal spot diameter (**i**) within hexagonal microlens array in (**b**). Green bars are plotted for simulation results.

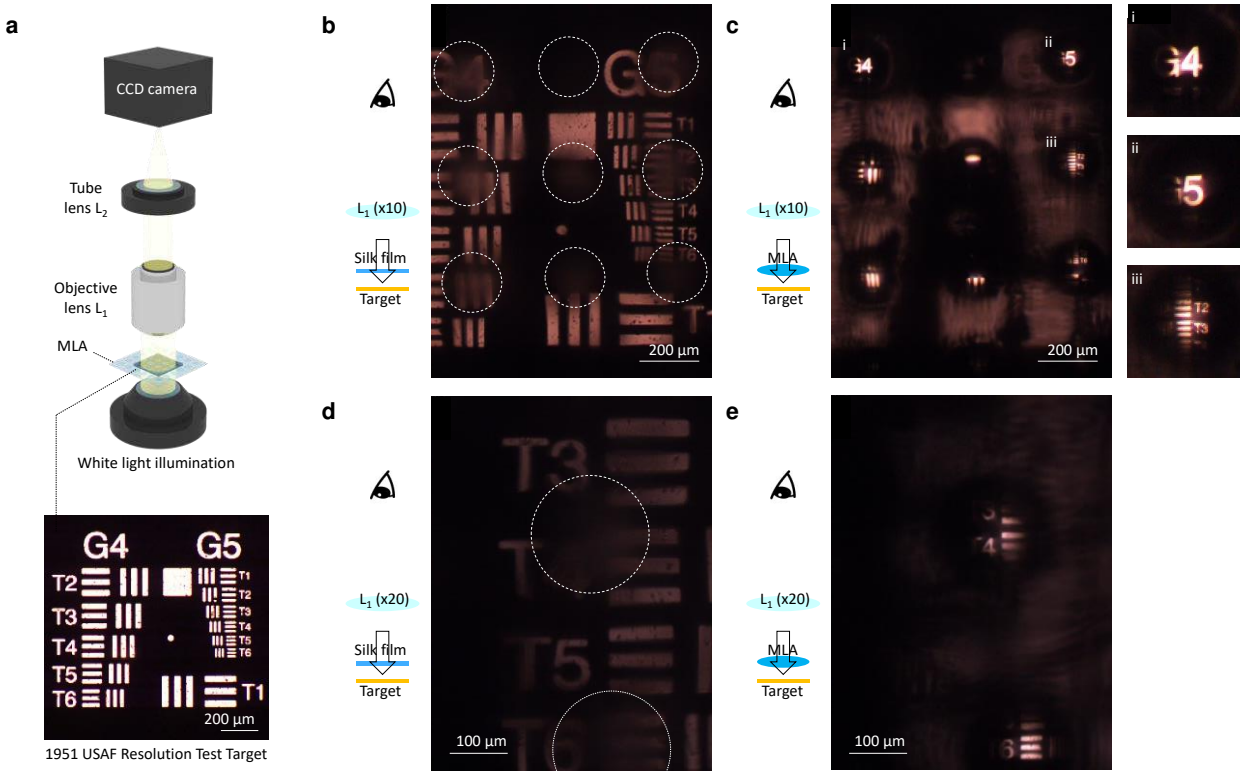

Figure 5. Optical imaging using silk microlens array. a Schematic of the optical microscope imaging setup with the silk microlens array (top). 1951 USAF resolution test target (bottom). **b**, **c** Bright-field images generated through the planar surface (**b**) and the curved surface (**c**) of silk microlens. A low magnification (10×) objective lens was used for imaging. **d**, **e** Bright-field images generated through the planar surface (**d**) and the curved surface (**e**) of silk microlens. A high magnification (20×) objective lens was used for imaging.

Table 1. Optical and structural properties of the silk microlens array

Material		Silk
Lens shape		Plano-convex
Deformability		Flexible
Parameters	Base width [μm]	200
	Height [μm]	36.6
	Radius of curvature [μm]	152.6
	Surface Roughness (RMS) [nm]	1.53
	Focal length (experiment) [μm]	265
	Focal length (simulation) [μm] @ROC = 150 μm	262.4
	Focal length (theory) [μm] @ROC = 150 μm	269.5
	Spot width (experiment) [μm]	2.89
	Spot width (simulation) [μm]	2.6
	Numerical aperture (NA)	0.35